Supporting Information

From aggregation-caused quenching to aggregation-induced delayed fluorescence: the impact of substituent effect

Yuqi Liu, Lijuan wang*, Lin Xu and Yan Song

School of Material Science and Engineering, Harbin Institute of Technology at Weihai, 2 West Wenhua Road, Weihai, 264209, China.
*Email: wanglijuan@hit.edu.cn.

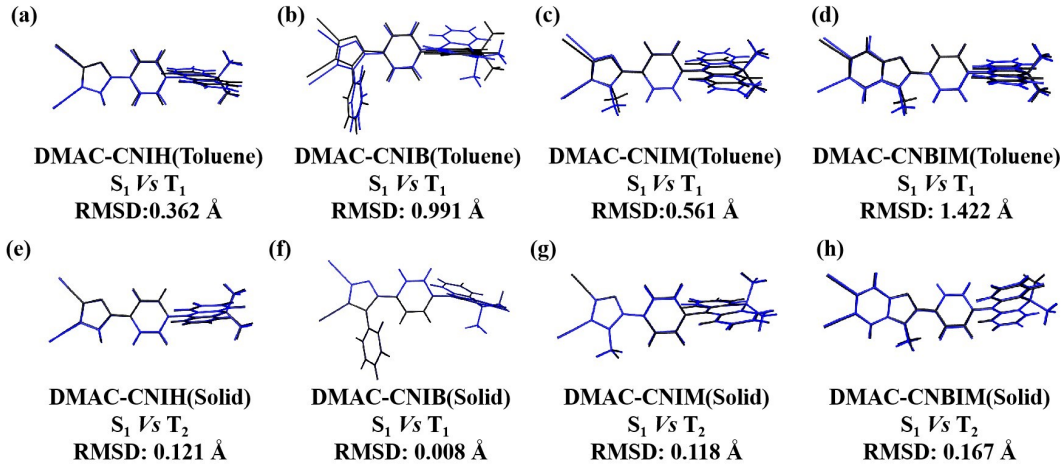

Figure S1 Geometrical structure comparisons and RMSD values (Å) between singlet state (black) and triplet state (blue) for DMAC-CNIH (a, e), DMAC-CNIB (b, f), DMAC-CNIM (c, g) and DMAC-CNBIM (d, h) in toluene and solid states.

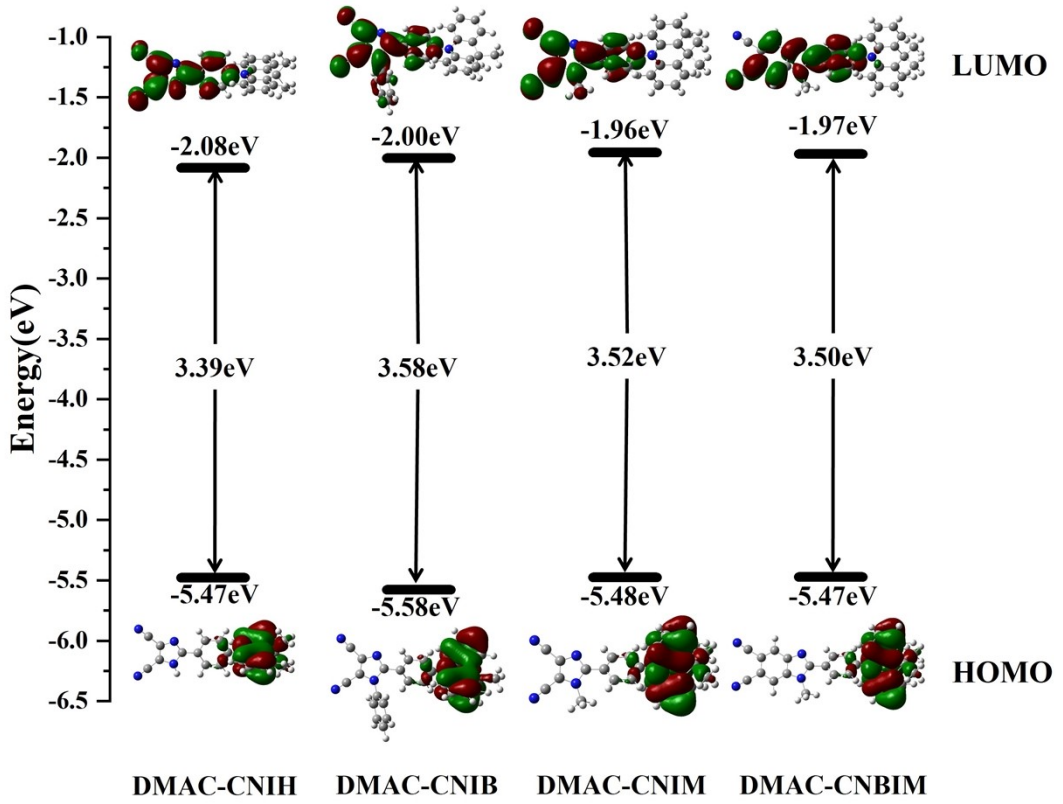

Figure S2 Distributions and energies of the frontier molecular orbitals for DMAC-CNIH, DMAC-CNIB, DMAC-CNIM and DMAC-CNBIM in toluene.

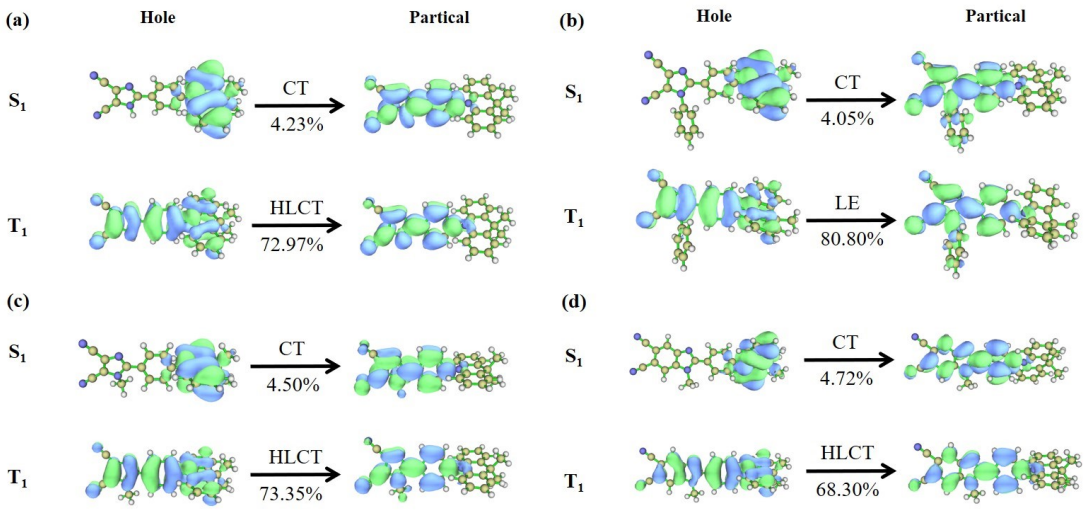

Figure S3 The natural transition orbital (NTO) of DMAC-CNIH (a), DMAC-CNIB (b), DMAC-CNIM(c) and DMAC-CNBIM (d) in toluene (the values are the component of localized excitation in the transitions).

Table S1 Emission wavelengths (nm) of the investigated molecules calculated by different basis sets with m06 functional in solid states.

Basis sets	DMAC-CNIH	DMAC-CNIB	DMAC-CNIM	DMAC-CNBIM
6-31G(d)	531	577	461	506
6-31G(d, p)	528	576	461	506
6-311G(d)	517	567	455	503
6-311G(d, p)	513	564	454	503
Exp.	517	500	479	502

Table S2 The oscillator strengths (f), the K_r (calculated by MOMAP and Einstein equation[a], s^{-1}), K_{nr} from S_1 to S_0 states (s^{-1}), the effective K_{ISC} and K_{RISC} between singlet and triplet states (s^{-1}), the prompt fluorescence (PF) efficiency (Φ_{PF})[b] and the delayed fluorescence quantum efficiency (Φ_{TADF})[b] based on the calculated K_r using MOMAP and Einstein equation in toluene and solid states, respectively.

	DMAC-CNIH		DMAC-CNIB		DMAC-CNIM		DMAC-CNBIM	
	toluene	crystal	toluene	crystal	toluene	crystal	toluene	crystal
f	0.0089	0.0026	0.0105	0.0001	0.0088	0.0020	0.0127	0.0008
K_r(MOMAP)	6.69×10^{3}	7.40×10^{5}	9.21×10^{3}	2.81×10^{4}	2.22×10^{4}	5.82×10^{5}	2.38×10^{4}	3.79×10^{5}
K_r(Einstein)	2.47×10^{6}	7.68×10^{5}	3.00×10^{6}	2.55×10^{4}	2.64×10^{6}	7.70×10^{5}	3.60×10^{6}	2.53×10^{5}
K_{nr} ($S_1\rightarrow S_0$)	1.01×10^{10}	6.34×10^{9}	1.50×10^{10}	1.13×10^{6}	1.52×10^{10}	8.83×10^{5}	1.47×10^{10}	4.74×10^{8}
K_{ISC} (S→T)	3.50×10^{3}	7.96×10^{7}	3.49×10^{3}	2.94×10^{7}	7.04×10^{3}	8.68×10^{8}	2.01×10^{3}	2.09×10^{7}
K_{RISC}(T→S)	5.24×10^{3}	1.68×10^{3}	3.26×10^{3}	5.86×10^{6}	6.84×10^{3}	6.09×10^{8}	2.00×10^{3}	1.27×10^{6}
Φ_{PF}(Einstein)	2.28×10^{-13}	4.33×10^{-7}	1.43×10^{-13}	1.02×10^{-3}	6.74×10^{-13}	1.73×10^{-3}	2.22×10^{-13}	5.11×10^{-4}
Φ_{TADF}(Einstein)	8.40×10^{-11}	1.50×10^{-6}	4.66×10^{-11}	1.78×10^{-2}	8.01×10^{-11}	3.86×10^{-1}	3.36×10^{-11}	2.25×10^{-5}
Φ_{PF}(MOMAP)	6.60×10^{-7}	1.15×10^{-4}	6.15×10^{-7}	9.21×10^{-4}	1.46×10^{-6}	6.69×10^{-4}	1.62×10^{-6}	7.65×10^{-4}
Φ_{TADF}(MOMAP)	2.28×10^{-13}	1.45×10^{-6}	1.43×10^{-13}	2.34×10^{-2}	6.74×10^{-13}	3.97×10^{-1}	2.22×10^{-13}	3.37×10^{-5}

[a]The Einstein spontaneous emission equation used to calculate K_r is written as $K_r = \frac{f\Delta E_{fi}^2}{1.499}$.

[b]The Φ_{PF} and Φ_{TADF} are calculated by the following equations: $\Phi_{PF} = \frac{K_r}{K_r + K_{nr+K_{ISC}}}$; $\Phi_{TADF} = \frac{\Phi_{ISC}\Phi_{RISC}}{1-\Phi_{ISC}\Phi_{RISC}}\Phi_{PF}$.

Table S3 The calculated electronic transition dipole moments (unit: Debye) from S_1 to S_0 state for DMAC-CNIH, DMAC-CNIB, DMAC-CNIM and DMAC-CNBIM in toluene and solid states.

DMAC-CNIH		DMAC-CNIB		DMAC-CNIM		DMAC-CNBIM	
Toluene	Solid	Toluene	Solid	Toluene	Solid	Toluene	Solid
0.0508	0.5439	0.0440	0.1345	0.0719	0.4446	0.0843	0.2887

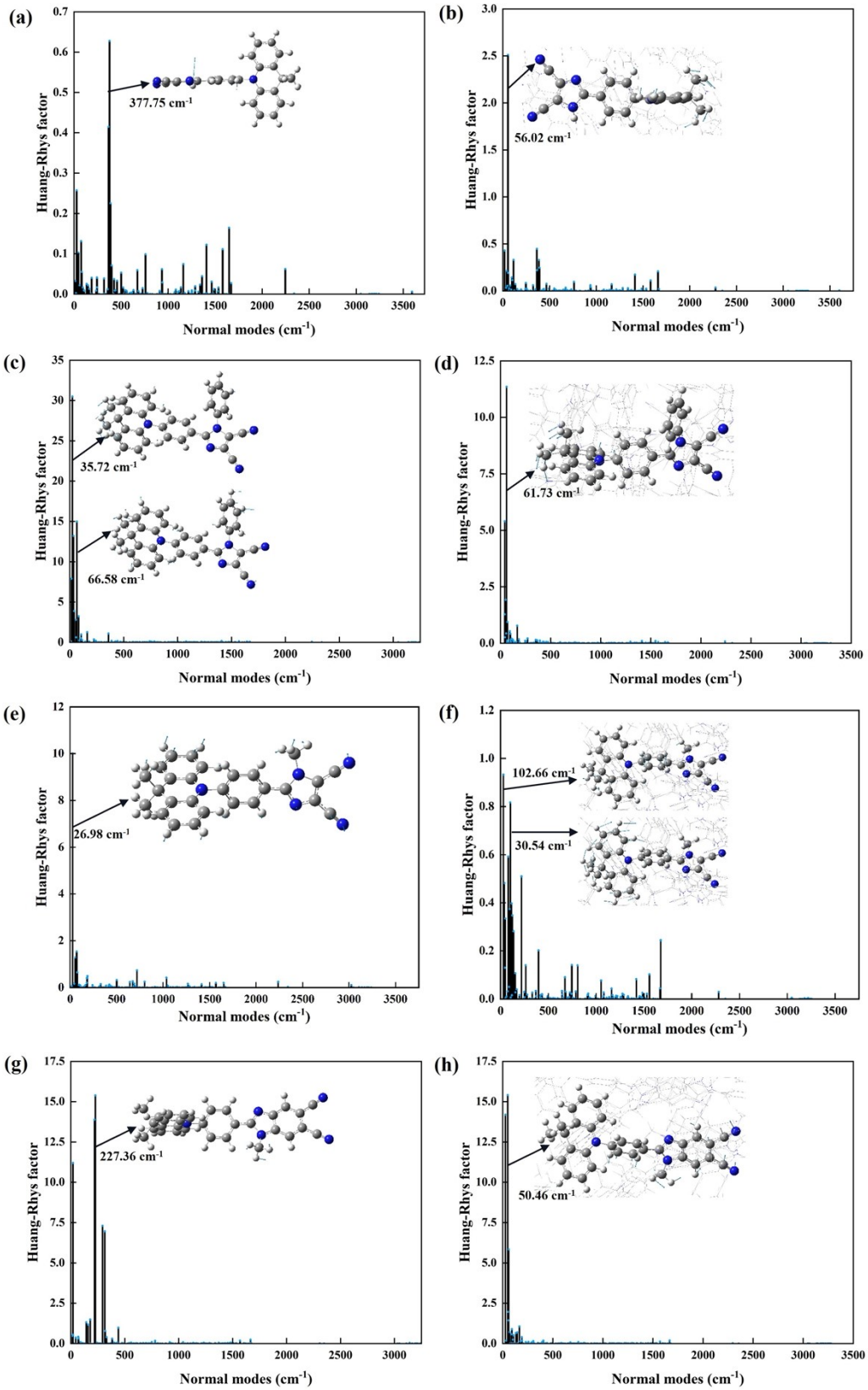

Figure S4 Calculated HR factors versus the normal mode frequencies from S_1 to S_0 state in both toluene (a, c, e, g) and solid (b, d, f, h) states for DMAC-CNIH (a, b), DMAC-CNIB (c, d), DMAC-CNIM (e, f) and DMAC-CNBIM (g, h). The vibration modes contributed the most are inserted.

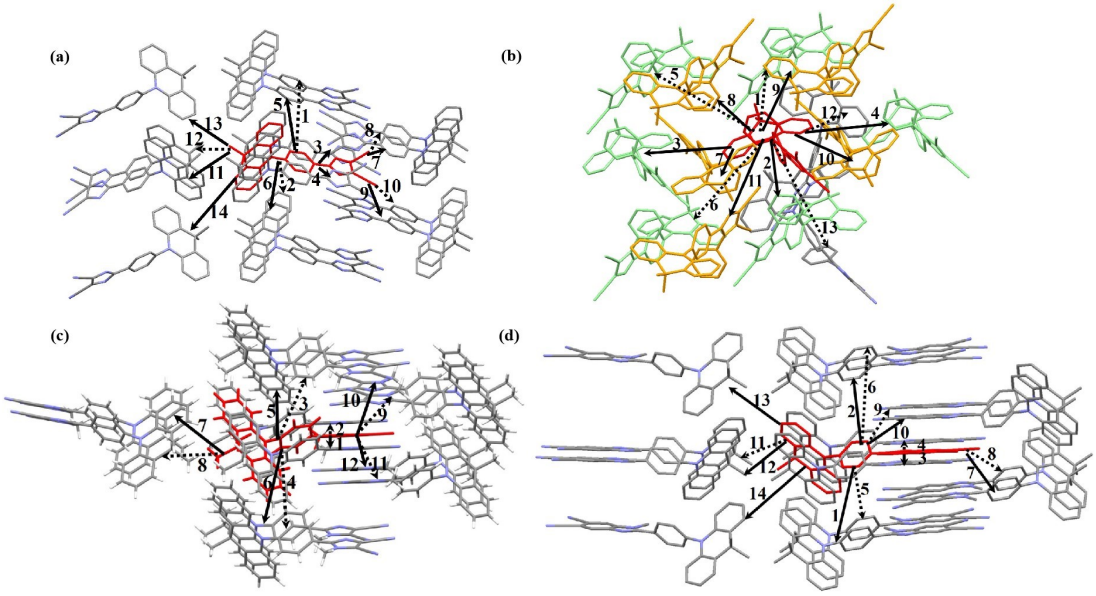

Figure S5 Main charge hopping pathways of DMAC-CNIH (a), DMAC-CNIB (b), DMAC-CNIM (c) and DMAC-CNBIM (d).

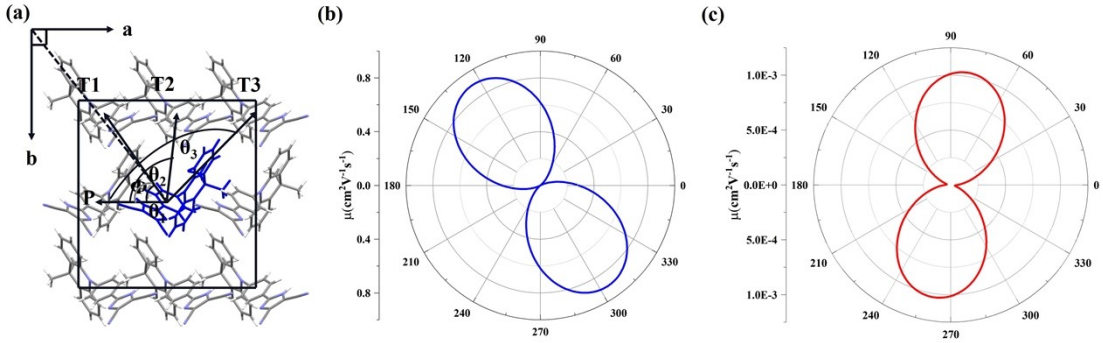

Figure S6 (a) Illustration of projecting angle-dependent hopping paths to a transistor channel in the *ab* plane and the calculated angle resolved anisotropic hole (b) and electron (c) mobilities of DMAC-CNIH.

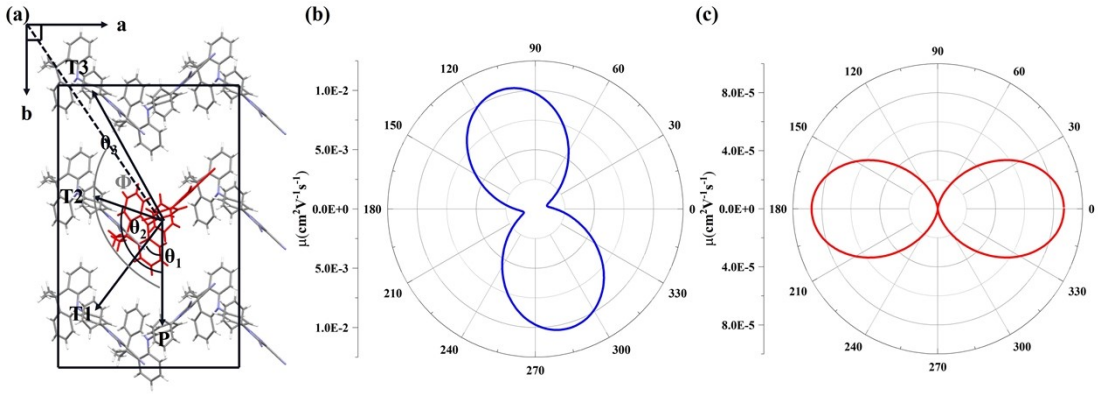

Figure S7 (a) Illustration of projecting angle-dependent hopping paths to a transistor channel in the *ab* plane and the calculated angle resolved anisotropic hole (b) and electron (c) mobilities of DMAC-CNIB.

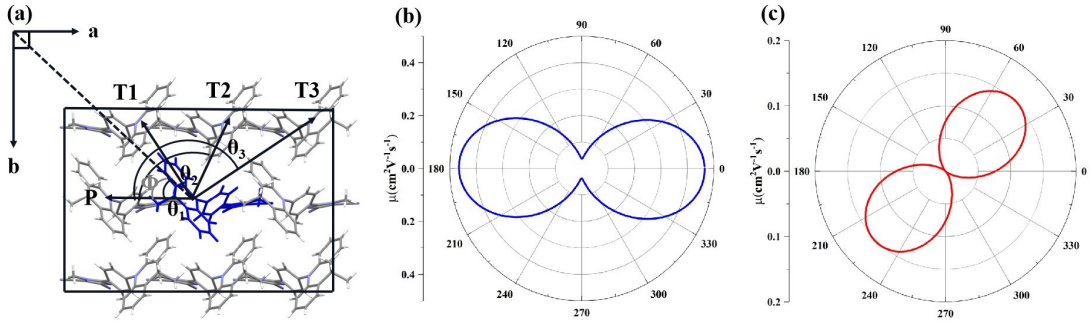

Figure S8 (a) Illustration of projecting angle-dependent hopping paths to a transistor channel in the *ab* plane and the calculated angle resolved anisotropic hole (b) and electron (c) mobilities of DMAC-CNIM.